Monthly Notices of the ROYAL ASTRONOMICAL SOCIETY

MNRAS **446,** 254–263 (2015) doi:10.1093/mnras/stu1967

The discrepancy in the mid-infrared continuum and the features of polycyclic aromatic hydrocarbons for *Spitzer* and *Herschel* SWIRE-field galaxies

Yi-Nan Zhu★ and Hong Wu

Key Laboratory of Optical Astronomy, National Astronomical Observatories, Chinese Academy of Sciences, Beijing 100012, China

Accepted 2014 September 19. Received 2014 September 17; in original form 2014 January 17

ABSTRACT

On the basis of observations by *Spitzer* and *Herschel*, we present and analyse the correlations between various monochromatic infrared (IR) luminosities for star-forming galaxies, selected from two northern *Spitzer* Wide-area InfraRed Extragalactic Survey (SWIRE) fields. The 24- and 70-μm luminosities (L[24] and L[70]), which are dominated by the continuum of very small grains (VSGs) and warm dust in thermal equilibrium, respectively, correlate tightly with ongoing star formation. The contribution from cool dust excited by evolved stars also increases as the wavelength increases in the far-infrared (FIR) wavelength range. The spectral features of ionized polycyclic aromatic hydrocarbons (PAHs) around rest-frame 8 μm are excited by the moderated radiation field related to evolved stars as well, rather than by the intensive radiation field related to young stars. Even though the carriers of PAHs could be treated as types of VSG with a smaller scale, the radiation condition between PAHs and classic VSGs seems to be significantly different. The formulae to calculate the total infrared luminosity $L_{\rm TIR}$ using L[8(dust)] and L[24] are re-scaled and we find that the L[8(dust)] (L[24]) formula likely underestimates (overestimates) $L_{\rm TIR}$ for galaxies with unusualcurrent star formation activity.

Key words: stars: formation – galaxies: starburst – infrared: galaxies.

1 INTRODUCTION

Dust emission heated by ultraviolet (UV) and optical photons dominates the infrared (IR) output for the majority of galaxies. Since the beginning of the Universe, about half of the bolometric emission of galaxies has been transported to the mid- (MIR) to far-infrared (FIR) (Hauser & Dwek 2001). Since celestial MIR and FIR photons suffer serious extinction when they run into the atmosphere surrounding us, observations above the absorbers (such as some types of molecule like water and carbon dioxide) are essential for IR astronomy. Since the successful launch of the *Infrared Astronomical Satellite* (*IRAS*) in 1983, more advanced space-based infrared telescopes have been launched, such as the *Infrared Space Observatory* (*ISO*: Kessler et al. 1996), *Spitzer Space Telescope* (Werner et al. 2004), *AKARI* (Murakami et al. 2007), *Herschel Space Observatory*[1] (Pilbratt et al. 2010) and the *Wide-field Infrared Survey Explorer* (*WISE*: Wright et al. 2010).

Dust is considered to form in the outer atmosphere of evolved stars and is then ejected out to interstellar space by stellar winds or some types of supernova. So far, many models have been proposed to scale the emission of dust (see e.g. Mathis & Whiffen 1989; Deśert, Boulanger & Puget 1990) and one of them is the silicate–graphite model (Mathis, Rumpl & Nordsieck 1977; Draine & Lee 1984). Recently, on the basis of *Spitzer* observations, a new version of the silicate–graphite model was demonstrated by Draine & Li (2007). This model contains different grain species, including silicate and graphite and polycyclic aromatic hydrocarbons (PAHs: Léger & Puget 1984; Puget & Léger 1989), the abundance and size distribution of which were derived to fit the average IR spectral energy distribution (SED) and reproduce the average extinction curve of the Milky Way. Since then, this model has been revised by some studies, such as the work of Galliano et al. (2011), who used *Spitzer* and *Herschel* images of the Large Magellanic Cloud (LMC) to restrict the behaviour of diverse dust grains.

Without consideration of the dust emission heated by active galactic nuclei (AGNs), the longer-wavelength FIR luminosity (>100 μm) of a galaxy is generally dominated by emission of dust in thermal equilibrium with a temperature of about 15–20 K, which will be treated as cool dust throughout this article, while the shorter-wavelength FIR luminosity (<100 μm) is dominated by dust in thermal equilibrium with a temperature higher than 30 K, which is

★ E-mail: zyn@bao.ac.cn

[1] *Herschel* is an ESA space observatory with science instruments provided by European-led Principal Investigator consortia and with important participation from NASA.

normally referred to as warm dust. The MIR continuum (<30 μm) comes from the emissions of very small grains (VSGs: Cesarsky et al. 2000) heated stochastically by single UV photons released by young stars in star formation regions.

The MIR continuum is also characterized by some broad emission features (Gillett, Forrest & Merrill 1973; Willner et al. 1977), which are realized to be from PAHs. In recent years, an understanding of the emissions of PAHs has developed based on the observations of *ISO* and *Spitzer* and a tight correlation between the emissions of PAHs and cool dust has been found and studied (Haas, Klaas & Bianchi 2002; Boselli, Lequeux & Gavazzi 2004; Bendo et al. 2006, 2008; Lu & Helou 2008). Low metallicities and the presence of AGNs could lead to the weakening of PAH emission (Siebenmorgen, Krügel & Spoon 2004; Verma et al. 2005; Weedman et al. 2005; Draine et al. 2007; Wu et al. 2007; Engelbracht et al. 2008). In a previous work (Zhu et al. 2008), on the basis of the *Spitzer* Wide-area InfraRed Extragalactic Survey (SWIRE: Lonsdale et al. 2003), we also found two tight correlations between 24 μm versus 70 μm luminosities and 8 μm versus 160 μm luminosities, respectively.

Because of the complication and diversity of IR emission, Dale & Helou (2002) employed three Multiband Imaging Photometer for *Spitzer* (MIPS: Rieke et al. 2004) bands, using 24-, 70- and 160-μm fluxes to compute the total IR luminosity ($L_{\rm TIR}$). Nevertheless, for current IR facilities, the sensitivity and angular resolution decrease gradually with increasing wavelength. Hence in most cases we can only use MIR photometry, such as 8- or 24-μm, to estimate $L_{\rm TIR}$. On the basis of *Spitzer* observations, Boquien et al. (2010) demonstrated that both metallicity and star formation intensity can influence the accuracy of the estimation of $L_{\rm TIR}$ if only one or two IR waveband photometries are used. Adding the observations of *Herschel*, Galametz et al. (2013) recalibrated the correlations between $L_{\rm TIR}$ and various monochromatic IR luminosities, then presented the discrepancy between the $L_{\rm TIR}$ derived from SED fitting and that found by scaling monochromatic IR luminosities. They also showed that the discrepancy was a function of IR colour, while the IR colour was sensitive to current star formation.

In this work, we will add the *Herschel* photometries in order to investigate the correlations between various monochromatic IR luminosities. The structure of the article is as follows. We describe the construction of our sample and the estimation of multi-wavelength luminosities in Section 2. The major results as regards correlation analysis are presented in Section 3. Some discussion and a summary of this work are given in Sections 4 and 5, respectively. Throughout this article, we have adopted a ΛCDM cosmology with $\Omega_{\rm m} = 0.3$, $\Omega_\Lambda = 0.7$ and $H_0 = 70\,{\rm km\,s^{-1}\,Mpc^{-1}}$.

2 DATA REDUCTION

2.1 SDSS data

Because we need the spectral redshift to calculate the distance and luminosities for IR-selected galaxies, first we downloaded a series of processed catalogues from the Max Planck Institute for Astrophysics (MPA) website,[2] then merged them together. These catalogues contain 927 552 sources included in the spectral sample of Data Release Seven (DR7) of the Sloan Digital Sky Survey (SDSS: York et al. 2000). Besides raw data, the MPA–Johns Hopkins University (JHU) team has also derived some physical quantities, such as spectral redshift, emission-line fluxes, stellar masses and metallicities. The data reduction has been detailed by Kauffmann et al. (2003), Tremonti et al. (2004) and Salim et al. (2007). It should be noted that the galaxies in the MPA–JHU catalogues are not restricted to those compiled as the main galaxy sample (Strauss et al. 2002). Some extended selected criteria have been adopted by the MPA–JHU team and a specific description of these selected criteria can be found on their website.[2]

2.2 *Spitzer* data

The *Spitzer* SWIRE is the largest extragalactic survey programme among the six *Spitzer* cycle-1 legacy programmes. This survey contains six regions, with a total field of ∼49 deg^2. Because of the limitations of the coverage of SDSS and *Herschel*, just two northern SWIRE fields, Lockman Hole (centre: 14 41 00, +59 25 00) and ELAIS–N1 (centre: 16 11 00, +55 00 00) are used in this work. The MIR and FIR photometric catalogues have been supplied to the public by the SWIRE team. We downloaded these catalogues from the InfraRed Science Archive (IRSA) website using the General Catalog Query Engine.[3] These catalogues can also be found and downloaded from the SWIRE team's website.[4] For each field of SWIRE, there are three photometric catalogues on the IRSA website: four *Spitzer* Infrared Array Camera (IRAC: Fazio et al. 2004) bands (3.6–8 μm) and MIPS 24 μm have been merged together, while the other two catalogues contain MIPS 70- and 160-μm band photometries respectively.

We cross-matched the IRAC/24-μm catalogue with the SDSS catalogue with a radius of 3 arcsec. After removing the repeated-crossing sources, 941 galaxies were left. Before cross-matching with the 70- and 160-μm photometries, we first calculated statistics for their astrometric precision: the mean values of 1σ position uncertainty are 1.5 and 3.5 arcsec for the 70- and 160-μm detected sources, respectively. We then used the 941 galaxies in the optical–MIR catalogue to match the 70- and 160-μm catalogues with radii of 4.5 and 10.5 arcsec, the 3σ position uncertainties. Finally, there were 253 optical–MIR galaxies that have both 70- and 160-μm detectable fluxes. It should be noted that the telescope-limited resolution of *Spitzer* is 18 and 40 arcsec at MIPS 70 and 160 μm, much larger than the cross-matching radius we have used. Inevitably, in order to improve the accuracy of our sample, the completeness of the sample has been sacrificed and we must have lost many FIR sources.

2.3 *Herschel* data

The *Herschel* Multi-tiered Extragalactic Survey (HERMES: Oliver et al. 2012) is one of the key programmes awarded on the *Herschel* Space Observatory as a Guaranteed Time survey. HERMES has mapped a set of separated fields in the sky with the Spectral and Photometric Imaging REceiver (SPIRE: Griffin et al. 2010) at 250, 350 and 500 μm (Levenson et al. 2010; Zemcov et al. 2013). Two fields in their second data release (DR2), Lockman–SWIRE and ELAIS–N1–HerMES, could be matched with the northern *Spitzer* SWIRE field. We downloaded the band-merged xID catalogues released at the end of 2013 (DR2).[5] The photometries in DR2 have been improved significantly (Wang et al. 2014) compared with those

[2] http://www.mpa-garching.mpg.de/SDSS/DR7/

[3] http://irsa.ipac.caltech.edu/applications/Gator/

[4] http://swire.ipac.caltech.edu/swire/astronomers/data/

[5] http://hedam.oamp.fr/HerMES/release.php

in the first data release (DR1: Roseboom et al. 2010; Smith et al. 2012). In these band-merged xID catalogues, the fluxes at 350 and 500 μm were extracted at 250-μm positions. In order to extract the sources from the SPIRE image, a Gaussian-shaped Point Spread Function (PSF) with full width at half-maximum (FWHM) set to 18.15, 25.15 and 36.3 arcsec at 250, 350 and 500 μm, respectively, was used by the HERMES team. The σ of the Gaussian-shaped PSF at 250 μm is about 7.8 arcsec, which was employed by us as the radius to match with the SDSS–*Spitzer* catalogue. After matching, 185 sources were left. If we enlarge the matching radius to 23 arcsec, three times the radius we used above, there is a total of 188 *Herschel* sources left. Hence, for the *Herschel* sources, the completeness of our sample is about 98 per cent.

2.4 Sample selection

Weak AGN-hosting galaxies are very common in the local Universe (Ho, Fillipenko & Sargent 1997). AGNs can strengthen the MIR continuum and weaken PAH emission or even destroy the carriers (Wu et al. 2007). Therefore, the probable contribution from AGNs to MIR and FIR emission would introduce significant bias to the correlations between those monochromatic IR luminosities. In this study, the traditional Baldwin–Phillips–Terlevich (BPT) diagnostic diagram, [N II]/Hα versus [O III]/Hβ (Baldwin, Phillips & Terlevich 1981; Veilleux & Osterbrock 1987), was used to remove AGN and composite galaxies (starburst + AGN) (Kewley et al. 2006). Out of the 185 galaxies of our sample, 104 of them (with signal-to-noise ratios (S/N) of the four emission-line fluxes >3) could be treated as star-forming galaxies without contamination by AGNs and are illustrated in the left panel of Fig. 1. The dotted curve in this panel is from Kauffmann et al. (2003). We also plot Kewley et al. (2001)'s criteria as a dashed curve, which is usually treated as the upper limit of ratios of emission lines in H II regions excited by inside or nearby stars. The objects below the dotted line were classified as star-forming galaxies; the others were removed and could be classified as narrow-line AGNs or composite galaxies.

The right panel of Fig. 1 is the rest-frame *B*-band absolute magnitude (M_B) distribution of the 104 star-forming galaxies; M_B was calculated from the SDSS *g*- and *r*-band magnitudes according to Smith et al. (2002). If −18 mag is used as the border to distinguish dwarf galaxies (Thuan & Martin 1981), then we find that only one galaxy can be treated as a dwarf.

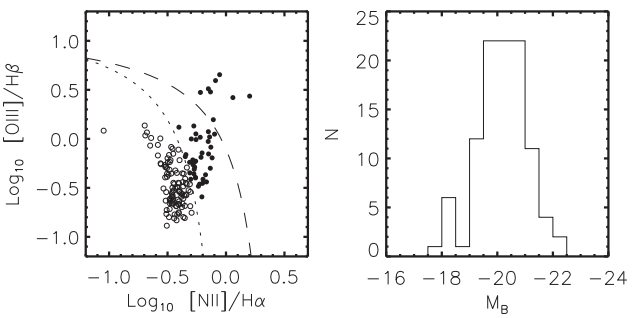

Figure 1. The left paned is the BPT diagnostic diagram: [N II]/Hα versus[O III]/Hβ. The criteria from Kauffmann et al. (2003) and Kewley et al. (2001) are illustrated as dotted and dashed curves, respectively. The objects below the dotted curve (open circles) are defined as star-forming galaxies. The right panel is the distribution of rest-frame absolute *B*-band magnitude for star-forming galaxies.

2.5 Estimation of monochromatic luminosities

We estimated the monochromatic IR luminosities by using spectral redshifts and the MIR and FIR fluxes provided by the above surveys. For the two *Spitzer* MIR bands, 8 and 24 μm, the fluxes from Kron photometry were adopted as total fluxes; for the two *Spitzer* FIR bands, 70 and 160 μm, point-response function (PRF) photometric fluxes were adopted; for the three *Herschel* FIR bands, 250, 350 and 500 μm, PSF photometric fluxes were adopted.

Besides the PAH features and VSG continuum, the photosphere of evolved stars could also contribute to the output at rest-frame 8 μm (Wu et al. 2005). Hence, we can only estimate a galaxy's 8-μm dust luminosity after reducing the stellar continuum component. A factor of 0.232 (Helou et al. 2004) was used to scale the starlight at 3.6 μm to that at 8 μm, with the assumption that the entire IRAC 3.6-μm band emission is from stellar emission and is based on the STARBURST99 synthesis model (Leitherer et al. 1999), assuming solar metallicity and a Salpeter initial mass function (IMF) between 0.1 and 120 $M_\odot$. Then, since the IRAC 8-μm band covers the complex PAH emission range, a more accurate SED model is needed to obtain a reliable MIR *K* correction. As in Zhu et al. (2008), we adopted a series of SEDs from Huang et al. (2007)'s two-component model, which is a linear combination of an old 'early-type' stellar population and a 'late-type' spiral disc population. The MIR colour [5.8]–[8.0] was used to select the best SED model and then the *K*-correction value was obtained. Huang et al. (2007)'s two-component model was used to perform *K* correction for the 3.6-μm band as well, which is usually treated as the tracer of stellar mass.

The contribution from the stellar continuum to the fluxes of the MIPS 24-μm band and the FIR bands can be neglected, since the emission of the evolved star photospheres decreases dramatically with increasing wavelength. A template MIR spectrum of a local H II galaxy NGC 3351 (from the *Spitzer* Infrared Nearby Galaxies Survey (SINGS): Kennicutt et al. (2003)), was convolved by using the spectral response curve of the MIPS 24-μm band to obtain the *K* correction at 24 μm.

In our sample, all galaxy fluxes at 70, 160 and 250 μm are larger than 3σ. With one exception, all source fluxes at 350 μm are larger than 3σ as well, while the S/N of the remaining galaxy's flux at 350 μm is 2.4 and we still employ it in this work. 61 of the galaxies in our sample have S/N of the flux at 500 μm larger than 3σ. For these 61 sources, the *K* corrections of five FIR waveband emissions (70, 160, 250, 350, 500 μm) were obtained by fitting fluxes in six bands (including 24 μm) with greybody emission and a MIR power-law continuum (Casey 2012). For the other 43 sources, only for four FIR wave bands (70, 160, 250, 350 μm) was *K* correction performed based on the SED fitting.

In this work, we use $L[a]$ to refer to the monochromatic luminosity (such that $L[24]$ is the 24-μm luminosity) and from here on the convention $L[a] = \nu L[a]$ is adopted for IR luminosity measurements. The monochromatic luminosities are in units of solar luminosity, which is 3.83×10^{33} erg s^{-1}. In our sample, the mean values of the 1σ error of the flux from 8–500 μm are 0.305, 0.714, 1.526, 2.885, 1.901, 6.387 and 15.487 per cent (the 61 sources with S/N of flux >3), respectively, corresponding to 0.002, 0.003, 0.007, 0.012, 0.008, 0.026 and 0.061 dex.

3 RESULTS

Fig. 2 shows the correlations between various monochromatic luminosities, including $L[8(\text{dust})]$, $L[24]$, $L[70]$, $L[160]$, $L[250]$, $L[350]$ and $L[500]$. The panels on the diagonal from top left to bottom right

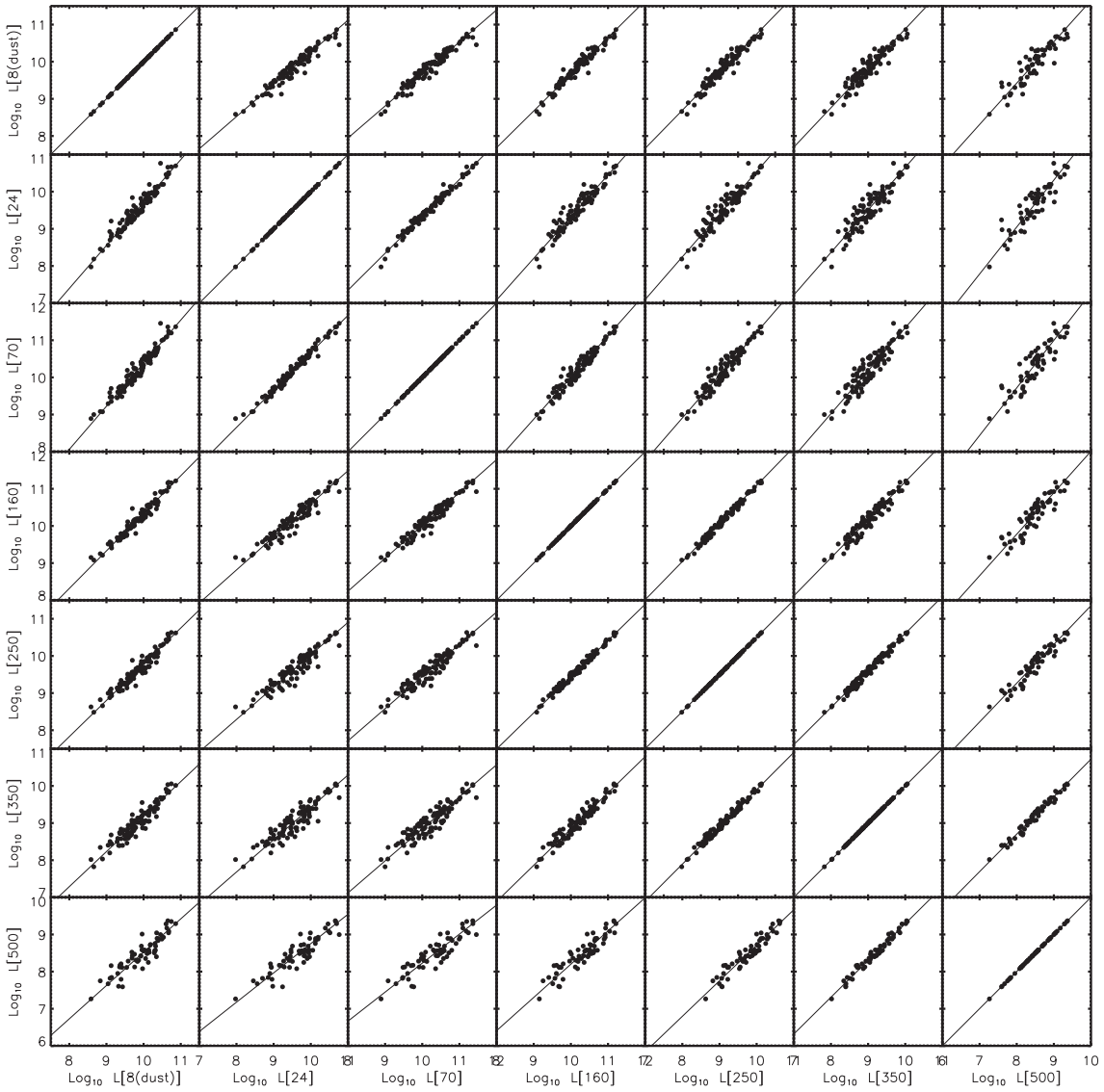

Figure 2. Correlations between various monochromatic IR luminosities for star-forming galaxies.

are the correlations between the monochromatic luminosities and themselves, so the figure is symmetrical. The number of galaxies in every panel is listed in Table 1. Using a two-variable regression, we obtain the best nonlinear fits ($\log_{10}(y) = a + b\log_{10}(x)$); these are shown as the solid line in each panel of Fig. 2 and the fitting parameters are listed in Table 1. The standard deviation of the fitting residuals and the coefficient of the Spearman rank-order correlation analysis are also listed in Table 1.

From Fig. 2, we can see that the star-forming galaxies in our sample show good correlations with various monochromatic luminosities. L[8(dust)] correlates more tightly with L[160] than with others. For L[24], the correlation with L[70] shows the largest Spearman rank-order correlation analysis coefficient (0.987); L[70] also tends to correlate with L[24] most tightly, while the correlations between L[24] and other monochromatic luminosities, even L[8(dust)], the other nearest waveband to 24 μm, are not as tight as the correlation between L[24] and L[70]. From L[70] to L[500], the coefficients of the Spearman rank-order correlation analysis between them and L[24] decrease monotonically with increasing wavelength (Lam et al. 2013), while the fitting errors increase gradually.

4 DISCUSSION

4.1 *L*[8(dust)] and cool dust emission

The monochromatic SPIRE luminosities, including L[250], L[350] and L[500], and even the *Spitzer* L[160] are clearly dominated by cool dust emission. L[8(dust)] correlates with monochromatic FIR luminosities more tightly, L[160] in particular, rather than with L[24] and L[70], indicating that the heating sources for the 8-μm (dust) and FIR emission may be the same. For a local star-forming galaxy, its 160-μm luminosity could be simply divided into two different parts: from H II regions, related to massive young hot stars, and from photo-dissociation regions (PDRs) or much cooler regions excited by the interstellar radiation field (ISRF), related to evolved stars. The dust emission related to the ISRF has been found to be prominent for the output of some very nearby galaxies at rest-frame 160 μm (Bendo et al. 2010, 2012). The rest-frame 8 μm (dust) luminosity of the local star-forming galaxies could also be divided into two different parts: the VSG continuum and spectral feathers from the C–C stretch and C–H bending of ionized PAHs. The

Table 1. Correlation coefficients between various monochromatic IR luminosities.

x (1)	*y* (2)	*N* (3)	*a* (4)	*b* (5)	*s* (6)	*c* (7)
L[8(dust)]	*L*[24]	104	−1.112 ± 0.080	1.072 ± 0.025	0.087	0.960
L[8(dust)]	*L*[70]	104	−1.219 ± 0.086	1.160 ± 0.027	0.092	0.971
L[8(dust)]	*L*[160]	104	0.228 ± 0.065	1.011 ± 0.020	0.068	0.974
L[8(dust)]	*L*[250]	104	0.027 ± 0.073	0.975 ± 0.023	0.078	0.963
L[8(dust)]	*L*[350]	104	−0.257 ± 0.090	0.943 ± 0.028	0.111	0.938
L[8(dust)]	*L*[500]	61	−0.447 ± 0.155	0.897 ± 0.049	0.139	0.898
L[24]	*L*[8(dust)]	104	1.038 ± 0.069	0.933 ± 0.022	0.081	0.960
L[24]	*L*[70]	104	0.016 ± 0.049	1.079 ± 0.016	0.061	0.987
L[24]	*L*[160]	104	1.199 ± 0.081	0.952 ± 0.026	0.107	0.945
L[24]	*L*[250]	104	0.833 ± 0.091	0.931 ± 0.029	0.121	0.924
L[24]	*L*[350]	104	0.223 ± 0.106	0.932 ± 0.034	0.141	0.898
L[24]	*L*[500]	61	0.332 ± 0.150	0.853 ± 0.048	0.145	0.872
L[70]	*L*[8(dust)]	104	1.051 ± 0.065	0.862 ± 0.020	0.079	0.971
L[70]	*L*[24]	104	−0.015 ± 0.044	0.927 ± 0.013	0.057	0.987
L[70]	*L*[160]	104	1.153 ± 0.063	0.886 ± 0.019	0.085	0.963
L[70]	*L*[250]	104	0.777 ± 0.079	0.867 ± 0.024	0.107	0.941
L[70]	*L*[350]	104	0.224 ± 0.100	0.862 ± 0.031	0.134	0.912
L[70]	*L*[500]	61	0.418 ± 0.146	0.781 ± 0.045	0.149	0.885
L[160]	*L*[8(dust)]	104	−0.225 ± 0.064	0.989 ± 0.020	0.067	0.974
L[160]	*L*[24]	104	−1.244 ± 0.093	1.049 ± 0.029	0.112	0.945
L[160]	*L*[70]	104	−1.243 ± 0.079	1.124 ± 0.024	0.096	0.963
L[160]	*L*[250]	104	−0.308 ± 0.037	0.975 ± 0.011	0.045	0.990
L[160]	*L*[350]	104	−0.923 ± 0.080	0.976 ± 0.025	0.093	0.958
L[160]	*L*[500]	61	−0.750 ± 0.157	0.895 ± 0.048	0.139	0.916
L[250]	*L*[8(dust)]	104	−0.028 ± 0.076	1.026 ± 0.024	0.080	0.963
L[250]	*L*[24]	104	−0.893 ± 0.106	1.074 ± 0.034	0.130	0.924
L[250]	*L*[70]	104	−0.888 ± 0.101	1.152 ± 0.032	0.123	0.941
L[250]	*L*[160]	104	0.316 ± 0.038	1.026 ± 0.012	0.046	0.990
L[250]	*L*[350]	104	−0.634 ± 0.044	1.003 ± 0.014	0.050	0.985
L[250]	*L*[500]	61	−0.863 ± 0.121	0.957 ± 0.038	0.104	0.951
L[350]	*L*[8(dust)]	104	0.272 ± 0.097	1.061 ± 0.032	0.118	0.938
L[350]	*L*[24]	104	−0.225 ± 0.119	1.072 ± 0.039	0.151	0.898
L[350]	*L*[70]	104	−0.228 ± 0.125	1.156 ± 0.041	0.155	0.912
L[350]	*L*[160]	104	0.946 ± 0.079	1.024 ± 0.026	0.096	0.958
L[350]	*L*[250]	104	0.632 ± 0.042	0.997 ± 0.014	0.050	0.985
L[350]	*L*[500]	61	−0.611 ± 0.068	0.990 ± 0.022	0.058	0.983
L[500]	*L*[8(dust)]	61	0.508 ± 0.178	1.114 ± 0.060	0.155	0.898
L[500]	*L*[24]	61	−0.369 ± 0.194	1.170 ± 0.066	0.170	0.872
L[500]	*L*[70]	61	−0.535 ± 0.216	1.281 ± 0.073	0.191	0.885
L[500]	*L*[160]	61	0.838 ± 0.177	1.117 ± 0.060	0.156	0.916
L[500]	*L*[250]	61	0.902 ± 0.124	1.045 ± 0.042	0.109	0.951
L[500]	*L*[350]	61	0.617 ± 0.066	1.010 ± 0.023	0.058	0.983

Note: Columns (1)–(2): names of multi-λ luminosities; column (3): the number of sample galaxies (after excluding dwarf galaxies) used for the fitting procedures; columns (4)–(5): the coefficients a and b of the nonlinear fit: $\log_{10}(y) = a + b\log_{10}(x)$, where all the luminosities are in units of $L_{\odot}$; column (6): the standard deviation s of the fitting residuals; column (7): the coefficient r of the Spearman rank-order correlation analysis.

continuum of VSGs is connected with ongoing star formation (see the next subsection). Although the carriers of PAHs could be considered as types of VSG with smaller scale (∼20 Å), the excitation for the PAH features and VSG continuum could definitely be different. The obvious decrease of PAH emission in low-metallicity galaxies has been detected and hard or intensive radiation may be responsible for this decrease (Engelbracht et al. 2005, 2008; Hogg et al. 2005; OHalloran et al. 2006; Madden et al. 2006; Wu et al. 2007; Galametz et al. 2009; Khramtsova et al. 2013). If this hypothesis is true, the ionized PAHs should be fragile.

From these considerations, PAHs should tend to settle in PDRs instead of H II regions, since PDRs are dominated by the ISRF and could shield intense UV photons (Tielens 2008). In order to check this hypothesis, it is necessary to search for the probable coincidence of the distributions of PAHs and the ISRF. The ISRF can be traced by 'middle-aged' or old stars. In this work, we use *L*[3.6], the rest-frame IRAC 3.6-μm luminosity, to represent the ISRF. The rest-frame 3.6-μm emissions can be used to compute the total stellar mass in galaxies without strong AGNs (Li et al. 2007; Cao et al. 2008), since the emission in this wavelength range

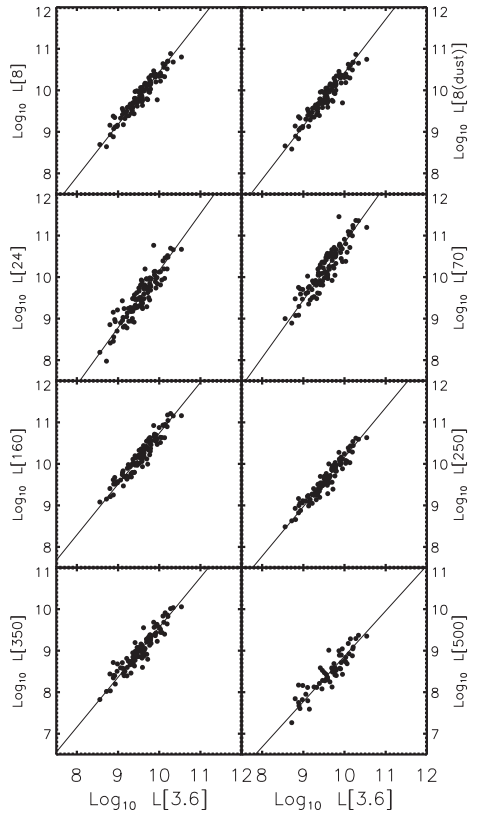

Figure 3. Correlations between 3.6 μm and the other monochromatic IR luminosities for star-forming galaxies.

is dominated by photons from the photospheres of red giants or supergiants, such as (post-) asymptotic giant branch ((p-) AGB) stars (Zhu et al. 2010; Wen et al. 2013).

The correlations between L[3.6] and other monochromatic luminosities are illustrated in Fig. 3. L[8] and L[8(dust)] represent the rest-frame 8-μm luminosities without and with stellar continuum subtraction. The best nonlinear fits using a two-variable regression are plotted as solid lines in all panels and the fitting parameters are listed in Table 2. The correlations of L[3.6] versus L[250] and L[3.6] versus L[160] are the tightest, then the correlations of L[3.6] versus L[8] and L[3.6] versus L[8(dust)]. The cool dust continuum dominating L[160] and L[250] is unambiguously related to evolved stars. Therefore, the MIR features of the C–C stretch and C–H bending of ionized PAHs seem to relate to evolved stars as well, excited by a moderate ISRF rather than by intensive radiation fields. This conclusion is the same as previous findings (Haas et al. 2002; Boselli et al. 2004; Bendo et al. 2006, 2008; Lu & Helou 2008; Boquien et al. 2011). Slater et al. (2011) demonstrated weaker PAH emission in some active H II regions in the Large Magellanic Cloud compared with evolved ones and some PAH emission outside galactic discs has even been detected in some nearby galaxies (Engelbracht et al. 2006; Irwin & Madden 2006; Kaneda et al. 2010). Recently, by using *Herschel*'s data, some researchers also discovered that the 8-μm emission is consistent with heating by the diffuse interstellar medium (Calapa et al. 2014; Ciesla et al. 2014; Lu et al. 2014). Accordingly, compared with other monochromatic MIR luminosities dominated by the VSG continuum instead of PAH features, L[8(dust)] seems not to be a good star formation tracer for star-forming galaxies in the local Universe, particularly for galaxies with weak star formation activity, in which the fraction of emission from H II regions is significantly small (Wu et al. 2005, 2007; Zhu et al. 2008).

Additionally, L[350] shows good correlation with L[3.6]. However, the correlation between L[500] and L[3.6] is the worst among all the correlations in Table 2. A submillimetre excess has also been found in some nearby galaxies based on *Herschel* observations (Auld et al. 2013). The excess is usually accredited to radiation from cold dust, the temperature of which is lower than 10 K (Skibba et al. 2012). In this work, however, on the basis of available data, we cannot determine the fraction of cold dust for 500-μm emission. In Fig. 4, we plot the correlation between L[500] (after K correction) and the value extrapolated from other band observation luminosities (from 24–350 μm); the right panel of Fig. 4 is their ratio as a function of B-band absolute magnitude. We could see that, compared with the extrapolated 500-μm luminosity, L[500] has no apparent enhancement, which leads to the conclusion that cold dust emission may be needless for the galaxies in our sample. This could also be due to the absence of dwarfs in our sample, while a submillimetre excess has often been found in local low-metallicity dwarf galaxies (Bolatto et al. 2000; Galliano et al. 2005, 2011). Furthermore, the thermal emission of cold dust is not the only possible explanation for the submillimetre excess (Dale et al. 2012). Other explanations, such as spinning dust (Bot et al. 2010), could enhance the submillimetre emission as well.

4.2 L[24] and warm dust emission

Fig. 2 shows that the correlation between L[24] versus L[70] is tighter than the rest. Traditionally, L[70] is thought to be dominated by the warm dust continuum, while L[24] is considered to come from VSGs heated stochastically by single UV photons emitted by young hot stars. Therefore, it is necessary to check the correlations between monochromatic IR luminosities and the star formation rate (SFR).

Table 2. Correlation coefficients between 3.6 μm and monochromatic IR luminosities.

x	y	N	a	b	s	c
(1)	(2)	(3)	(4)	(5)	(6)	(7)
L[3.6]	versus L[8]	104	-2.175 ± 0.103	1.261 ± 0.033	0.105	0.943
L[3.6]	versus L[8(dust)]	104	-2.422 ± 0.112	1.284 ± 0.036	0.112	0.940
L[3.6]	versus L[24]	104	-2.838 ± 0.149	1.286 ± 0.048	0.153	0.904
L[3.6]	versus L[70]	104	-3.005 ± 0.164	1.383 ± 0.053	0.164	0.909
L[3.6]	versus L[160]	104	-1.502 ± 0.103	1.224 ± 0.033	0.101	0.951
L[3.6]	versus L[250]	104	-1.759 ± 0.091	1.192 ± 0.029	0.090	0.955
L[3.6]	versus L[350]	104	-2.456 ± 0.105	1.202 ± 0.034	0.108	0.934
L[3.6]	versus L[500]	61	-2.061 ± 0.186	1.092 ± 0.060	0.141	0.892

Note: Column definitions are the same as in Table 1.

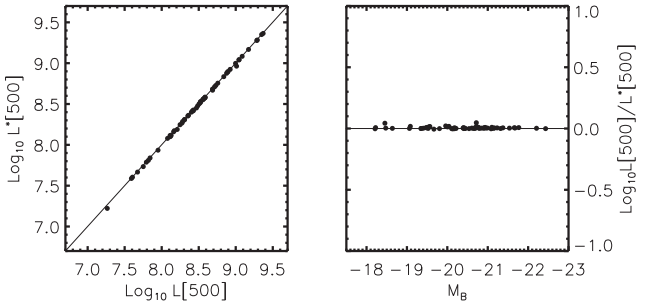

Figure 4. Left: the correlation between $L[500]$ (after K correction) and $L^*[500]$, extrapolated from other band observation luminosities (from 24–350 μm). Right: the correlation between M_B and $L[500]/L^*[500]$.

Here, we use the Hα luminosity as the star formation rate tracer (Kennicutt 1998). The optical Hα emission suffers from dust extinction from both the Milky Way and the host galaxy. The foreground Galactic extinction was first corrected by assuming Cardelli, Clayton & Mathis (1989)'s extinction curve and $R_V = 3.1$. Intrinsic extinction correction was performed, based on the colour excess $E(B-V)$, which was acquired from the Balmer decrement $F_{H\alpha}/F_{H\beta}$ (Calzetti 2001). The SDSS optical spectra were taken with 3 arcsec diameter fibres; thus the measured Hα emission fluxes were only from the central regions for most low-redshift galaxies and a corresponding aperture correction is needed. We adopted the method by Hopkins et al. (2003) and used their equation (A2) to obtain the Hα luminosity of the whole galaxy (Zhu et al. 2008). The aperture correction to Hα luminosities was performed based on the assumption that the distributions of Hα emission in galaxies are similar to those of continuum (SDSS $-$ r) emission.

Fig. 5 shows the correlations between L[Hα] and monochromatic IR luminosities. The best nonlinear fits using a two-variable regression are plotted as solid lines and the fitting parameters are listed in Table 3. Apparently, L[24] and L[70] correlate with L[Hα] most tightly in Fig. 5. The scatter in the correlations between L[8(dust)] versus L[Hα] is larger than those for L[24] versus L[Hα] and L[70] versus L[Hα]. From L[160] to L[500], the correlations with L[Hα] decrease gradually, similarly to the tendencies with L[24] and L[70] (see Section 3). Hence, compared with other monochromatic IR luminosities, L[24] and L[70] should be considered as good SFR tracers, consistent with previous findings such as the works of Calzetti et al. (2005, 2007, 2010), Wu et al. (2005) and Kennicutt et al. (2007, 2009).

Now we employ L[24] as the SFR tracer and show the ratios between L[24] and the remaining six monochromatic IR luminosities as a function of L[24] in Fig. 6. The ratios have been shifted to around zero by subtracting the statistical mean value in each panel. In Fig. 6, we can see that, excepting L[24]/L[70], the remaining five ratios cannot stay as approximate constants with increasing SFR. Therefore, compared with 24 and 70 μm, the fraction of emission related to young stars is smaller in other FIR wave bands and even in 8 μm (dust). Then, by using the luminosity ratio of 24 to 3.6 μm as the tracer of specific star formation rate (SSFR), we demonstrate the correlations between SSFR and the ratios between L[24] and the remaining six monochromatic luminosities in Fig. 7. The panels in Fig. 7 are similar to the corresponding ones in Fig. 6, except that the SFR is replaced by the SSFR on the x-axis and the scatter in each panel is smaller. It is clear in Fig. 7 that the ratios between dust related and not related to current star formation increase gradually with star formation activity, which indicates that overestimation of

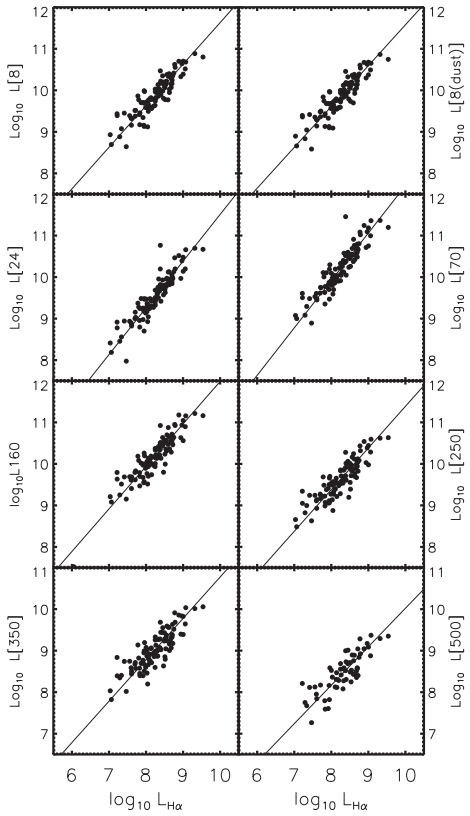

Figure 5. Correlations between Hα and monochromatic IR luminosities for star-forming galaxies.

SFR would be inevitable if we only calculate SFR based on the FIR (>100 μm) luminosity, particularly for galaxies with significant emission from cool dust (Lam et al. 2013).

4.3 Estimation of L_{TIR} from L[8(dust)] and L[24]

Current star formation could bias the estimation of L_{TIR}. This case has been discussed in detail using Key Insights on Nearby Galaxies: a Far-Infrared Survey with *Herschel* (KINGFISH: Kennicutt et al. 2012) galaxies (Galametz et al. 2013). Here, we recalibrate the correlations between L[8(dust)] and L[24] with L_{TIR}. L_{TIR} was obtained from fitting fluxes in six bands (excluding 8 μm, because of the undefined contributions from PAHs) with greybody emission and a MIR power-law continuum. The procedures were supplied by Casey (2012) and Casey et al. (2013). Only sources with detectable fluxes larger than 3σ in the 500-μm band were selected. The final sample includes 61 galaxies.

L[8(dust)] and L[24] are plotted against L_{TIR} in Fig. 8. The best nonlinear fits using a two-variable regression are plotted as solid lines. Table 4 lists the fitting parameters. The dotted lines in Fig. 8 represent the fitting correlations for nearby galaxies from SINGS and KINGFISH obtained by Galametz et al. (2013). We find that the best nonlinear fit of L[24] versus L_{TIR} in this work is fully consistent with the corresponding result in Galametz et al. (2013). However, the slope of our nonlinear fit of L[8(dust)] versus L_{TIR} is a little steeper than that in Galametz et al. (2013); this discrepancy could be due to the different galaxy populations in these two samples: the galaxies in Galametz et al. (2013) are all nearby ones, even including some optical dwarfs, but there is a lack of IR-luminous

Table 3. Correlation coefficients between Hα and monochromatic IR luminosities.

x (1)	y (2)	N (3)	a (4)	b (5)	s (6)	c (7)
L[Hα]	versus L[8]	104	1.617 ± 0.122	1.001 ± 0.042	0.151	0.909
L[Hα]	versus L[8(dust)]	104	1.739 ± 0.123	0.984 ± 0.042	0.148	0.909
L[Hα]	versus L[24]	104	0.789 ± 0.100	1.049 ± 0.034	0.129	0.936
L[Hα]	versus L[70]	104	0.781 ± 0.112	1.142 ± 0.038	0.146	0.933
L[Hα]	versus L[160]	104	1.745 ± 0.123	1.024 ± 0.042	0.161	0.898
L[Hα]	versus L[250]	104	1.351 ± 0.130	1.003 ± 0.044	0.169	0.878
L[Hα]	versus L[350]	104	0.802 ± 0.144	0.997 ± 0.049	0.187	0.850
L[Hα]	versus L[500]	61	0.749 ± 0.211	0.927 ± 0.072	0.202	0.813

Note: The definition of columns are the same as in Table 1.

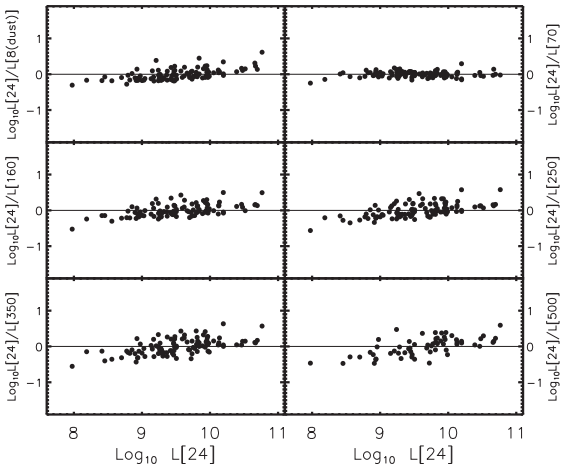

Figure 6. Correlations between L[24] and the ratios of L[24] to other monochromatic luminosities. The ratios have been shifted to around zero by subtracting the statistical mean value in each panel. As the wavelength of the denominator increases, the mean value is 0.305, 0.668, 0.652, 0.090, −0.512 and −1.176, respectively.

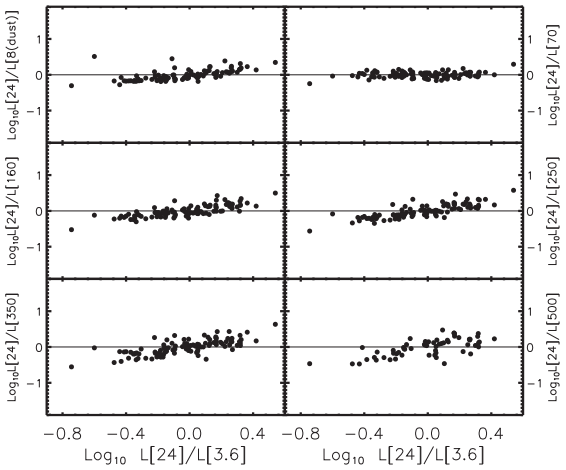

Figure 7. Correlations between SSFR and the ratios of L[24] to other monochromatic luminosities. The SSFR was represented by the ratio of 24 to 3.6 μm luminosities. As in Fig., the ratios have been shifted to around zero by subtracting the statistical mean value in each panel.

galaxies (located at the top right in the left panel of Fig. 8), which tend to have higher SFRs and lower ratios of L[8(dust)] to $L_{\rm TIR}$.

In order to check the discrepancy of fittings in left panel of Fig. 8 caused by the different galaxy populations, we show the $L_{\rm TIR}$ ratios

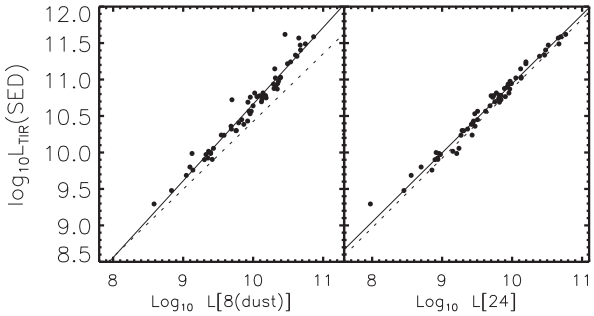

Figure 8. Correlations between MIR luminosities and $L_{\rm TIR}$ from SED fitting. The best nonlinear fits are illustrated as solid lines. The dotted lines are the nonlinear fits in Galametz et al. (2013).

between the value (represented as $L^*_{\rm TIR}$ in this subsection) estimated using monochromatic MIR luminosities (both L[8(dust)] and L[24]) and the value from SED fitting, as a function of SFR and SSFR, in Fig. 9. Here, the SFR is represented by L[24] and the SSFR is represented by the luminosity ratio between rest-frame 24 and 3.6 μm. In Fig. 9, a solid circle denotes $L^*_{\rm TIR}$ estimated using nonlinear fitting parameters (Table 4); a cross denotes $L^*_{\rm TIR}$ estimated using the equations in Galametz et al. (2013). In Fig. 9, we find that $L^*_{\rm TIR}$ values calculated based on the formulae derived by us are larger than $L^*_{\rm TIR}$ values calculated based on the formulae presented by Galametz et al. (2013), particularly when utilizing L[8(dust)] to estimate $L^*_{\rm TIR}$. Additionally, we see, for galaxies with higher SFR or higher SSFR, that the ratio between $L^*_{\rm TIR}$ derived from L[8(dust)] (using both our and Galametz et al. (2013)'s formulae) and $L_{\rm TIR}$ from SED fitting descends gradually, which indicates again that L[8(dust)] is not as good as L[24] and L[70] at tracing ongoing star formation. For galaxies with higher SSFR, the ratio between $L^*_{\rm TIR}$ derived from L[24] and $L_{\rm TIR}$ from SED fitting increases slightly, but this tendency cannot be seen in the bottom left panel. One of the probable explanations is that galaxies with higher SSFR, rather than higher SFR, lack cool dust grains, so the overestimation of $L^*_{\rm TIR}$ derived from L[24] is unavoidable; another possible explanation is that the radiation field of whole galaxies has been dominated by young hot stars for those galaxies with higher SSFR. Consequently, for galaxies with intense star formation, if we only employ the MIR luminosity dominated by the emission related to young stars to compute the total IR luminosity, overestimation seems to be inevitable, whilst if we employ the formulae derived on the basis of the monochromatic MIR luminosity influenced significantly by the spectral features of PAHs, underestimation of the total IR luminosity would not be impossible.

Table 4. Correlation coefficients between L[8(dust)] and $L_{\rm TIR}$ from SED fitting.

x	y	N	a	b	s	c
(1)	(2)	(3)	(4)	(5)	(6)	(7)
L[8(dust)]	versus $L_{\rm TIR}$	61	0.149 ± 0.071	1.051 ± 0.022	0.062	0.980
L[24]	versus $L_{\rm TIR}$	61	1.467 ± 0.052	0.948 ± 0.016	0.051	0.987

Note: The definition of columns are the same as in Table 1.

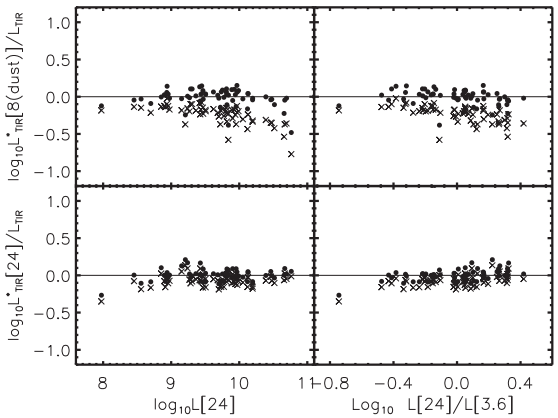

Figure 9. Comparison between $L^*_{\rm TIR}$ estimated using L[8(dust)] and L[24] and the $L_{\rm TIR}$ from SED fitting, as a function of SFR and SSFR, represented seperately by L[24] and the luminosity ratio of 24 to 3.6 μm. The solid circle in each panel denotesthe $L^*_{\rm TIR}$ estimated using the formulae derived by ourselves (the parameters are demonstrated in Table); a cross denotes the $L^*_{\rm TIR}$ estimated using the equations by Galametz et al. (2013).

5 SUMMARY

We present and analyse the correlations between L[8(dust)], L[24], L[70], L[160], L[250], L[350] and L[500] for a sample of galaxies selected from *Spitzer* and *Herschel* data in two northern SWIRE fields. The galaxies in our sample represent local star-forming galaxies, showing a lack of optical and IR dwarfs as well as ultraluminous infrared galaxies. The main results described in this article can be summarized as follows.

(1) The L[24] and L[70] of star-forming galaxies are found to be well correlated with each other, then correlated with extinction-corrected Hα luminosities. These correlations indicate the similarity of heating sources of VSGs and warm dust. Therefore, estimating SFRs using L[24] and L[70] would be more feasible than using other monochromatic IR luminosities. Nevertheless, only employing the monochromatic IR luminosities that are primarily relevant for young hot stars may overestimate $L_{\rm TIR}$.

(2) For FIR emission longer than 100 μm, the contributions from warm dust vanished gradually with increasing wavelength. Cool dust excited by the ISRF controls the emission in these FIR wave bands, especially for galaxies with quiescent star formation. Hence, a colour correction would be useful when obtaining the SFR using FIR (>100 μm) luminosities.

(3) L[8(dust)] is composed of a continuum of VSGs and characteristic spectral features of PAHs. L[8(dust)] is well correlated with FIR (>100 μm) luminosities, especially with L[160] and L[250]. We therefore suspect that the C–C stretch and C–H bending of ionized PAHs is mainly excited by the ISRF and the features of PAHs follow the cool dust emission, rather than warm dust or VSG emission related to star formation. L[8(dust)] could be used to derive the SFR, but may be not as good as L[24] and L[70]. We re-scale the correlations between $L_{\rm TIR}$ and L[8(dust)], but, for galaxies with higher SFR or SSFR, underestimation of $L_{\rm TIR}$ would be inevitable if only using L[8(dust)] or other monochromatic MIR luminosities dominated by the spectral features of PAHs.

ACKNOWLEDGEMENTS

We thank Caitlin M. Casey and her collaborators for helping us in revising their procedures for fitting IR SEDs and we thank the anonymous referee for constructive comments and suggestions. We thank Dr Z.-M. Zhou for smoothing the lauguage. We acknowledge Drs K. Xu, N.-Y. Lu, Z.-M. Zhou and Mam I Lam for advice and helpful discussions.

This project is supported by the National Natural Science Foundation of China (Grant number 11173030), the Ministry of Science and Technology of the People's republic of China through grant 2012CB821800 and 2014CB845705, and by NSFC grants 11225316, 11078017 and 10833006. This work is also supported by the Strategic Priority Research Program 'The Emergence of Cosmological Structures' of the Chinese Academy of Sciences, Grant No. XDB09000000. This project is also supported by the Strategic Priority Research Program "The Emergence of Cosmological Structures" of the Chinese Academy of Sciences, Grant No. XDB09000000.

This work is based on observations made with the *Spitzer* Space Telescope, which is operated by Jet Propulsion Laboratory of the California Institute of Technology under NASA Contract 1407. This research has made use of the NASA/IPAC Infrared Science Archive, which is operated by the Jet Propulsion Laboratory, California Institute of Technology, under contract with the National Aeronautics and Space Administration. We acknowledge the useful SWIRE catalogues from NASA/IPAC Infrared Science Archive.

Herschel is an ESA space observatory with science instruments provided by European-led Principal Investigator consortia and with important participation from NASA. This research has made use of data from the HerMES project (http://hermes.sussex.ac.uk/). HerMES is a Herschel Key Programme utilizing Guaranteed Time from the SPIRE instrument team, ESAC scientists and a mission scientist. HerMES has been described in Oliver et al. (2012). The HerMES data were accessed through the HeDaM data base (http://hedam.oamp.fr) operated by CeSAM and hosted by the Laboratoire d'Astrophysique de Marseille.

We acknowledge the useful SDSS data base and the MPA/JHU catalogues. Funding for the SDSS and SDSS-II has been provided by the Alfred P. Sloan Foundation, the Participating Institutions, the National Science Foundation, the US Department of Energy, the National Aeronautics and Space Administration, the Japanese Monbukagakusho, the Max Planck Society and the Higher Education Funding Council for England. The SDSS Web Site is http://www.sdss.org/. The SDSS is managed by the Astrophysical Research Consortium for the Participating Institutions. The Participating Institutions are the American Museum of Natural History, Astrophysical Institute Potsdam, University of Basel, University of Cambridge, Case Western Reserve University,

University of Chicago, Drexel University, Fermilab, the Institute for Advanced Study, the Japan Participation Group, Johns Hopkins University, the Joint Institute for Nuclear Astrophysics, the Kavli Institute for Particle Astrophysics and Cosmology, the Korean Scientist Group, the Chinese Academy of Sciences (LAMOST), Los Alamos National Laboratory, the Max-Planck-Institute for Astronomy (MPIA), the Max-Planck-Institute for Astrophysics (MPA), New Mexico State University, Ohio State University, University of Pittsburgh, University of Portsmouth, Princeton University, the United States Naval Observatory and the University of Washington.

REFERENCES

Auld R. et al., 2013, MNRAS, 428, 1880
Baldwin J. A., Phillips M. M., Terlevich R., 1981, PASP, 93, 5
Bendo G. J. et al., 2006, ApJ, 652, 283
Bendo G. J. et al., 2008, MNRAS, 389, 629
Bendo G. J. et al., 2010, A&A, 518, 65
Bendo G. J. et al., 2012, MNRAS, 419, 1833
Bolatto A. D., Jackson J. M., Wilson C. D., Moriarty-Schieven G., 2000, ApJ, 532, 909
Boquien M. et al., 2010, ApJ, 713, 626
Boquien M. et al., 2011, AJ, 142, 111
Boselli A., Lequeux J., Gavazzi G., 2004, A&A, 428, 409
Bot C. et al., 2010, A&A, 523, 20
Calapa M. D. et al., 2014, ApJ, 784, 130
Calzetti D., 2001, PASP, 113, 1449
Calzetti D. et al., 2005, ApJ, 633, 871
Calzetti D. et al., 2007, ApJ, 666, 870
Calzetti D. et al., 2010, ApJ, 714, 1256
Cao C., Wu H., Wang Z., Ho L.-C., Huang J.-S., Deng Z.-G., 2008, New Astron., 13, 16
Cardelli J. A., Clayton G. C., Mathis J. S., 1989, ApJ, 345, 245
Casey C. M., 2012, MNRAS, 425, 3094
Casey C. M. et al., 2013, ApJ, 761, 140
Cesarsky D., Lequeux J., Ryter C., Gérin M., 2000, A&A, 354, L87
Ciesla L. et al., 2014, A&A, 565, 128
Dale D. A., Helou G., 2002, ApJ, 576, 159
Dale D. A. et al., 2012, ApJ, 745, 95
Deśert F.-X., Boulanger F., Puget J. L., 1990, A&A, 237, 215
Draine B. T., Lee H. M., 1984, ApJ, 285, 89
Draine B. T., Li A., 2007, ApJ, 657, 810
Draine B. T. et al., 2007, ApJ, 663, 866
Engelbracht C. W. et al., 2005, ApJ, 628, L29
Engelbracht C. W. et al., 2006, ApJ, 642, L127
Engelbracht C. W. et al., 2008, ApJ, 678, 804
Fazio G. G. et al., 2004, ApJS, 154, 10
Galametz M. et al., 2009, A&A, 508, 645
Galametz M. et al., 2013, MNRAS, 431, 1956
Galliano F., Madden S. C., Jones A. P., Wilson C. D., Bernard J.-P., 2005, A&A, 434, 867
Galliano F. et al., 2013, A&A, 536, 88
Gillett F. C., Forrest W. J., Merrill K., 1973, ApJ, 183, 87
Griffin M. J. et al., 2010, A&A, 518, L3
Haas M., Klaas U., Bianchi S., 2002, A&A, 385, L23
Hauser M. G., Dwek E., 2001, ARA&A, 39, 249
Helou G. et al., 2004, ApJS, 154, 253
Ho L. C., Fillipenko A. V., Sargent W. L. W., 1997, ApJ, 487, 568
Hogg D. W. et al., 2005, ApJ, 624, 162
Hopkins A. M. et al., 2003, ApJ, 599, 971
Huang J.-S. et al., 2007, ApJ, 664, 840
Irwin J. A., Madden S. C., 2006, A&A, 445, 123
Kaneda H. et al., 2010, A&A, 514, 14
Kauffmann G. et al., 2003, MNRAS, 346, 1055
Kennicutt R. C., Jr, 1998, ARA&A, 36, 189
Kennicutt R. C. et al., 2003, PASP, 115, 928
Kennicutt R. C. et al., 2007, ApJ, 671, 333
Kennicutt R. C., Jr 2009, ApJ, 703, 1072
Kennicutt R. C., Jr et al., 2012, PASP, 123, 1347
Kessler M. F. et al., 1996, A&A, 315, L27
Kewley L. J., Heisler C. A., Dopita M. A., Lumsden S., 2001, ApJS, 132, 37
Kewley L. J., Groves B., Kauffmann G., Heckman T. M., 2006, MNRAS, 372, 961
Khramtsova M. S., Wiebe D. S., Boley P. A., Pavlyuchenkov Ya . N., 2013, MNRAS, 431, 2006
Lam M.-I., Wu H., Zhu Y.-N, Zhou Z.-M., 2013, Res. Astron. Astrophys., 13, 179
Léger A., Puget J. L., 1984, A&A, 137, L5
Leitherer C. et al., 1999, ApJS, 123, 3
Levenson L. et al., 2010, MNRAS, 409, L83
Li H.-N., Wu H., Cao C., Zhu Y.-N., 2007, AJ, 134, 1315
Lonsdale C. J. et al., 2003, PASP, 115, 897
Lu N.-Y., Helou G., 2008, in Chary R.-R., Teplitz H. I., Sheth K., eds, ASP Conf. Ser. Vol. 381, The Second Annual Spitzer Science Center Conference: Infrared Diagnostics of Galaxy Evolution. Astron. Soc. Pac., San Francisco, p. 46
Lu N.-Y. et al., 2014, preprint (arXiv:1410.3874)
Madden S. C., Galliano F., Jones A. P., Sauvage M., 2006, A&A, 446, 877
Mathis J. S., Whiffen G., 1989, ApJ, 341, 808
Mathis J. S., Rumpl W., Nordsieck K. H., 1977, ApJ, 217, 425
Murakami H. et al., 2007, PASJ, 59, 369
Oliver S. J. et al., 2012, MNRAS, 424, 1614
OHalloran B. et al., 2006, ApJ, 641, 795
Pilbratt G. L. et al., 2010, A&A, 518, L1
Puget J. L., Léger A., 1989, ARA&A, 27, 161
Rieke G. H. et al., 2004, ApJS, 154, 25
Roseboom I. G. et al., 2010, MNRAS, 409, 48
Salim S. et al., 2007, ApJS, 173, 267
Siebenmorgen R., Krügel E., Spoon H. W. W., 2004, A&A, 414, 123
Skibba R. A. et al., 2012, ApJ, 761, 42S
Slater C. T. et al., 2011, ApJ, 732, 98
Smith J. A. et al., 2002, AJ, 123, 2121
Smith A. J. et al., 2012, MNRAS, 419, 377
Strauss M. A. et al., 2002, AJ, 124, 1810
Thuan T. X., Martin G. E., 1981, ApJ, 247, 823
Tielens A. G. G. M., 2008, ARA&A, 46, 289
Tremonti C. A. et al., 2004, ApJ, 613, 898
Veilleux S., Osterbrock D. E., 1987, ApJS, 63, 295
Verma A., Charmandaris V., Klaas U., Lutz D., Haas M., 2005, Space Sci. Rev., 119, 355
Wang L. et al., 2014, MNRAS, 444, 2870
Weedman D. W. et al., 2005, ApJ, 633, 706
Wen X.-Q. et al., 2013, MNRAS, 433, 2946
Werner M. W. et al., 2004, ApJS, 154, 1
Willner S. P., Soifer B. T., Russell R. W., Joyce R. R., Gillett F. C., 1977, ApJ, 217, 121
Wright E. L. et al., 2010, AJ, 140, 1868
Wu H., Cao C., Hao C.-N., Liu F.-S., Wang J.-L., Xia X.-Y., Deng Z.-G., Young C. K. S., 2005, ApJL, 632, L79
Wu H., Zhu Y.-N., Cao C., Qin B., 2007, ApJ, 668, 87
York D. G. et al., 2000, AJ, 120, 1579
Zemcov M. et al., 2013, ApJ, 769, 31
Zhu Y.-N., Wu H., Cao C., Li H.-N., 2008, ApJ, 686, 155
Zhu Y.-N., Wu H., Li H.-N., Cao C., 2010, Res. Astron. Astrophys., 10, 329

This paper has been typeset from a TEX/LATEX file prepared by the author.